Desalination and Water Treatment
www.deswater.com
doi: 10.5004/dwt.2020.25584

187 (2020) 399–409
May

$FeVO_4$ nanoparticles synthesis, characterization and photocatalytic activity evaluation for the degradation of 2-chlorophenol

Asma Shafique[a], I.A. Bhatti[a], A. Ashar[a,b], M. Mohsin[a], Sheikh Asrar Ahmad[c], Jan Nisar[d], Tariq Javed[e,*], M. Iqbal[f,*]

[a]*Department of Chemistry, University of Agriculture, Faisalabad, 38040, Pakistan, emails: chemnceac@outlook.com (A. Shafique), ijazchem@yahoo.com (I.A. Bhatti), ambreenashar2013@gmail.com (A. Ashar), m.mohsin618@gmail.com (M. Mohsin)*
[b]*Department of Chemistry, Government College Women University, Faisalabad, 38040, Pakistan*
[c]*Department of Chemistry, Division of Science and Technology, University of Education Lahore, Vehari Campus, Pakistan, email: asrarchemist@ue.edu.pk (S.A. Ahmad)*
[d]*National Center of Excellence in Physical Chemistry, University of Peshawar, Peshawar, 25120, Pakistan, email: pashkalawati@gmail.com (J. Nisar)*
[e]*Department of Chemistry, University of Sahiwal, Sahiwal 57000, Pakistan, email: jtariqchemist@gmail.com (T. Javed)*
[f]*Department of Chemistry, The University of Lahore, Lahore, 53700, Pakistan, email: munawar.iqbal@chem.uol.edu.pk (M. Iqbal)*

Received 30 August 2019; Accepted 22 January 2020

ABSTRACT

Heterostructured nanoparticles are active under visible light and have gained much attention for the remediation of persistent organic pollutants under visible light irradiation. Iron vanadate ($FeVO_4$) was prepared by the co-precipitation technique and characterized by X-ray diffraction, scanning electron microscope, energy dispersive X-rays, and zeta particle sizer techniques. The particle size of $FeVO_4$ was in the range of 190–210 nm with maximum abundance at 150 nm. The particle was in a spherical shape and agglomerated form. The band-gap of $FeVO_4$ particles was 2.95 eV. Photocatalytic activity was evaluated by degrading 2-chlorophenol (2-CP) under solar light irradiation. The process variables, that is, catalyst dose, pH, initial concentration of CP, H_2O_2 concentration, and irradiation time are optimized using response surface methodology. At optimized conditions, up to 91% degradation of 2-CP was achieved and degradation was mentored by ultraviolet-visible spectroscopy and high-performance liquid chromatography analysis. The observed and predicted 2-CP degradation responses were in agreement with low residual values. Results revealed that $FeVO_4$ is active under solar light irradiation that could possibly be used for the treatment of wastewater containing toxic dyes.

Keywords: Heterostructured nanoparticle; Iron vanadate; photocatalytic activity; advance oxidation process; 2-chlorophenol

1. Introduction

Phenol and its derivatives are toxic and hazardous pollutants, which enter into the environment by various anthropogenic activities and used as disinfectant and preservation agents for fiber, paint, wood, and leather [1–3]. It is also used for the synthesis of pesticides, herbicides, fungicides, pharmaceuticals, insecticides, and dyes. Due to its toxicity, solubility, and stability in water, 2-CP containing water needs to be treated before being discharged into water bodies. Hence, wastewater needs to be treated and an advanced oxidation process based on photocatalyst is one of the promising techniques [4–10]. Different chemical, thermal, and biological methods are being used for the removal of 2-CP from water. The treatments like reverse osmosis, adsorption, coagulation, ultra-filtration, and precipitation produce secondary pollutants and also demand the post-treatment for proper functioning. Biological method needs longer

* Corresponding authors.

degradation time and microorganisms are sensitive to the environmental conditions and toxic by-products. All these conventional treatments are time-consuming, ineffective, and non-compatible with the environment [11–21].

In this regard, there is an urgent need to develop an innovative, facile, and environment-friendly method for water purification. The ultimate goal is to attain the complete mineralization of organic pollutants into carbon dioxide and water [22–24]. In this context, the advance oxidation process is a highly efficient technology [25,26]. These processes are accomplished by the *in situ* production of strong oxidizing species such as hydroxyl radical ($^{\bullet}OH$) and superoxide anion radical ($O_2^{\bullet-}$) which are responsible to trigger the free radical reaction to degrade the organic compound in an aqueous medium to harmless substances [13,27]. Heterogeneous photocatalysis is an advance oxidation process which is an efficient and promising approach for the degradation of the organic contaminants in the atmospheric and aquatic environment. For the photocatalytic degradation of pollutants, semiconductor-based photocatalysis is an efficient technique and has proved a real interest for the researchers due to its innovative, less expensive, and robust nature [28]. Semiconductor based photocatalysis involves the generation of electron and hole pair in valence and conduction band, respectively, by the excitation of electrons from the valence band to conduction band when the light of suitable energy equivalent to band-gap falls on the semiconductor material. Electron and hole pairs generated are responsible for the secondary redox reactions to degrade persistent organic pollutants. However, it has some limitations such as a large band-gap which requires photon of ultraviolet (UV) origin and thus limits the efficacy of the photocatalyst [29].

Different techniques are used to overcome the intrinsic limitations by reducing the size of photocatalytic materials at the nanoscale, formulation of composites at the nanoscale level, doping of materials with metals and non-metals and formation of metal-organic frameworks are useful to control band-gap of the photocatalysts [29,30]. For the degradation of organic pollutants, materials constitute a smaller band-gap and are active under visible light have dominant importance in heterogeneous photocatalysis. Inorganic compounds such as multi-metallic oxides of vanadates, tungstates, and molybdates having shorter band-gap are efficient for catalytic applications [29,31–33]. Orthovanadtes (AVO_4) based on transition metals are an important class of inorganic materials which have versatility in applications in several fields especially in catalysis. The large number of new compounds can be formed due to many stable oxidation states of the vanadium [25].

Vanadium has the ability to combine with metal ions due to variable oxidation state and vanadates emerged an important class of materials that have been used in diverse fields such as photocatalyst, lithium-ion batteries, water splitting, catalyst, supercapacitors, antibacterial, ion-exchange materials, luminescence, and photoluminescence device and gas sensors [34]. V_2O_5 has been successfully employed to fabricate a diverse type of heterostructured materials ($LaVO_4$, $EuVO_4$, and $BiVO_4$). V_2O_5 is a n-type semiconductor with narrow band-gap considered for using in photocatalytic degradation and water treatment. However, studies on $FeVO_4$/V_2O_5 to prepare heterostructured nanoparticles are rare and on the basis of band-gap tuning, their photocatalytic activity (PCA) can be enhanced. Different methods have been reported to synthesize iron vanadate ($FeVO_4$), that is, sol-gel, wet chemical, microwave, hydrothermal, solid-state, and precipitation [34].

Based on the aforementioned facts, $FeVO_4$, heterostructured nanoparticles were prepared by solution chemistry and characterized by X-ray diffraction (XRD), Scanning electron microscope (SEM), Energy dispersive X-rays (EDX), diffused reflectance spectroscopy (DRS), and Zeta particle sizer techniques. The PCA was evaluated by degrading 2-chlorophenol (2-CP, Fig. 1) under sunlight irradiation. The process variables, that is, catalyst dose, pH, the concentration of CP, H_2O_2 concentration, irradiation time were optimized using response surface methodology (RSM). Under optimized conditions rate constant of the photocatalytic reaction was determined and the efficiency of synthesized $FeVO_4$ was compared with commercial catalysts.

2. Material and methods

2.1. Chemicals and reagents

All the chemical reagents used were of analytical grade. Ferric nitrate [$Fe(NO_3)_3$], ammonium salts of vanadates, polyethylene glycol (PEG), ethylene, and ethanol were purchased from Sigma-Aldrich (St. Louis, United States). Commercial $FeVO_4$/C was purchased from Merck (Lincoln Ave, Rahway, United States) and is used without any purification and characterization. Ultrapure water of resistivity of 18.2 MΩ cm (at 25°C) was used for the preparation of solutions.

2.2. Synthesis procedure

For the fabrication of $FeVO_4$, the co-precipitation method was adopted as reported by Nithya et al. [35]. Ammonium metavanadate (NH_4VO_3) and $Fe(NO_3)_3$ were used as precursors. Iron nitrate (0.1 M) solution was prepared by dissolving 4.84 g/200 mL water and ammonium metavanadate (0.1 M) was prepared by dissolving 2.43 g/200 mL of water. NH_4VO_3 solution was heated at 75°C till a clear solution was obtained. Then, 5 mL of PEG was added and the solution was stirred for 30 min. Then, iron nitrate solution was mixed dropwise along with slow stirring. Yellowish-brown precipitates were appeared and the reaction was continued for 8 h. Precipitates were filtered and washed several times with water and ethanol and dried at 70°C. The synthesized $FeVO_4$/S was characterized by SEM, EDX, XRD, Particle Sizer, and DRS techniques.

Table 1
Experimental design showing the process variable and their levels

Name	Symbols	Range and levels		
		Low (–1)	Middle (0)	High (+1)
Catalyst load, g/L	A	1	2	3 or 1.5
pH	B	3	6	9
2-CP conc., mg/L	C	10	20	30
H_2O_2, %	D	3	5	7

2.3. Photo-catalytic activity

The PCA was evaluated by degrading 2-CP as a function of catalyst load, pH, 2-CP concentration, and H_2O_2 concentration, whose level is shown in Table 1 and responses are presented in Table 2. Central composite design (CCD) was employed for statistical modeling of the degradation process. After mixing the 2-CP and catalysts and adjusting the conditions (pH adjustment and H_2O_2 addition), the mixture was kept in the dark for 30 min in order to ensure the adsorption-desorption of the catalyst surface. The photocatalytic experiments were done under artificial solar radiation (150 W D65 tubes) in a closed reactor. After stipulated time intervals, 2 mL sample was drawn, filtered by Millipore filter and analyzed for dye residual concentration of 2-CP. Blank experiments were also performed under similar conditions to evaluate the pure effect of photolysis, H_2O_2 and a commercial sample of $FeVO_4$. Triplicate degradation experiments were run under ambient conditions (25°C) and data thus obtained is averaged. The 2-CP percentage of degradation was estimated by employing the relation shown in Eq. (1). Where C_i is the initial concentration of 2-CP and C_f is the concentration of 2-CP after photocatalytic treatment.

$$2-\text{CP degradation}\left(\%\right)=\left[\frac{C_i-C_f}{C_i}\right]\times 100 \quad (1)$$

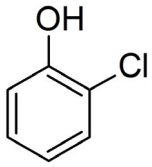

Fig. 1. Structure of 2-chlorophenol used for PCA evaluation.

2.4. Spectrophotometric and HPLC analysis

The 2-CP degradation was monitored by HPLC and ultraviolet-visible spectroscopy (243 nm). For HPLC analysis, HPLC (Hewlett-Packard, Alexandria, United States, Series 1100) equipped with a UV detector at 243 nm and C18 column was used. Acetonitrile and water were used as eluent *A* and *B* with a volume ratio of 70:30, which were filtered and degasified and used as a mobile phase with a flow rate of 1 cm^3/min with injection volume 1 μL.

3. Results and discussion

3.1. Characterization

The $FeVO_4$ was characterized by EDX, XRD, Particle size analysis, and SEM techniques. EDX analysis was carried out in order to determine the elemental composition and percentage purity of $FeVO_4$. EDX analysis indicated the presence of V, O, and Fe in the material synthesized (Fig. 2). The intensities of the peaks can also be correlated with the percentage of respective elements. Hosseinpour-Mashkani et al. [36] also reported similar results for $FeVO_4$

Table 2
Experimental layout showing the predicted and actual 2-CP degradation values

Run	Experimental conditions				Degradation (%) age	
	Catalyst load (g/L)	pH	2-Chlorophenol (mg/L)	H_2O_2 (%)	Actual	Predicted
1	3	9	30	3	35	34.77
2	3	9	10	3	63	62.73
3	3	3	30	7	38	37.76
4	1	9	10	7	54	53.73
5	3	3	10	7	70	69.74
6	1	3	30	3	21	20.76
7	1	9	30	7	36	35.77
8	1	3	10	3	48	47.73
9	0.32	6	20	5	42	42.35
10	3.68	6	20	5	43	43.36
11	2	0.96	20	5	46	46.35
12	2	11.10	20	5	47	47.35
13	2	6	3.18	5	91	91.398
14	2	6	36.82	5	47	47.31
15	2	6	20	1.64	50	50.35
16	2	6	20	8.37	66	66.36
17	2	6	20	5	77	76.03
18	2	6	20	5	76	76.04
19	2	6	20	5	76	76.04
20	2	6	20	5	75	76.03
21	2	6	20	5	77	76.03

synthesized by the ultrasonic approach. XRD pattern of $FeVO_4$ is shown in Fig. 3. XRD pattern is attributed to the pure form of $FeVO_4$, which is $FeVO_4.nH_2O$ and in line with JCPDS card no. 27-0257. Average crystallite size (L) of $FeVO_4$ was calculated using the relation shown in Eq. (2) [37].

$$L = \frac{0.9\lambda}{\beta\cos\theta} \tag{2}$$

where λ = 1.54 Å (λ_{max} for X-rays), k = 0.9 (shape constant), $\theta = 2\theta/2$ (Bragg's angle of diffraction), β = FWHM (in radian; full width at half maximum peak intensity) and the average crystallite size of $FeVO_4$ was found to be 35 nm. These findings are in line with reported studies, that is, Deng et al. [38] investigated the influence of calcination temperature on the crystallinity of iron vanadate and it was observed that at 100°C broad peaks were observed, which showed the formation of amorphous compound. It was revealed that clear and intense XRD diffraction peaks were obtained by increasing the calcination temperature up to 500°C to 600°C, respectively, and concluded that gradual transformation occurs from amorphous to crystalline nature. Similarly, Nithya et al. [35] studied the effects of surfactants, reaction time and calcination temperature on the crystallinity of $FeVO_4$ prepared by the co-precipitation method. XRD confirmed the single phase of $FeVO_4$ with triclinic structure and high crystallinity. In this study, optimum temperature and reaction time furnished the crystalline sample and by increasing the temperature, the phase was changed. It was also depicted that the addition of surfactants increased the calculated X-ray density of nanocrystallites and was comparable with the standard reported value of 3.647 g/cm^3 (PDF No. 38–1372).

SEM analysis was employed to investigate the morphology and surface properties of $FeVO_4$ and results are shown in Fig. 4. The $FeVO_4$ has a fluffy texture and highly porous structure ranging in the size of 100–200 nm. These small granules and fluffy textured $FeVO_4$ has great potential for catalytic activity. According to previous reports, the drying process at low temperature furnished less crystalline structure and more amorphous contents lead toward the fluffy shaped structure. It has been observed that at temperature lower than 60°C more dispersed shape and greater agglomeration effects were seen, while compact and small grains having an average size of 150 nm were obtained at high temperature. Zeta particle sizer was used to assess the particle size of $FeVO_4$ and results revealed that particle size was in 100–200 nm range with maximum distribution at 150 nm (Fig. 5). The morphology has greater efficacy in catalytic activity, which enables the charge carriers to move to the surface by providing the channel to the electrons transfer. The morphology and size of as prepared $FeVO_4$ can be effected by the synthesis conditions, that is, Chan et al. [39] prepared flake-like structure through precipitation method and particle size was up to 8 μm and base exerted strong influence on the morphology of NPs. Ozturk and Soylu [40] also studied the effect of pH and surfactant on the morphology of $FeVO_4$, which was found dependent on the addition of surfactant. Ma et al. [41] also reported the controllable synthesis of porous $FeVO_4$ nanorods, which was found dependent on synthesis conditions.

Optical property of the $FeVO_4$ was exhibited by its sunlight harvesting capacity which was found in the visible region. Diffused reflectance spectra revealed the band-gap edge at 400 nm and an increase in absorption of solar radiation bellow 520 nm (Fig. 6a). The DRS values for reflectance (%R) were used to estimate the band energy as shown in Eq. (4b) using the Kubelka Munk equation [42]. The maximum absorbing capacity of the $FeVO_4$ revealed band-gap to be 2.95 eV.

3.2. PCA optimization for the degradation of 2-CP

The PCA of $FeVO_4$ was evaluated by degrading 2-CP as a modal compound. The process variables like the concentration of 2-CP, pH, H_2O_2 concentration, and catalyst

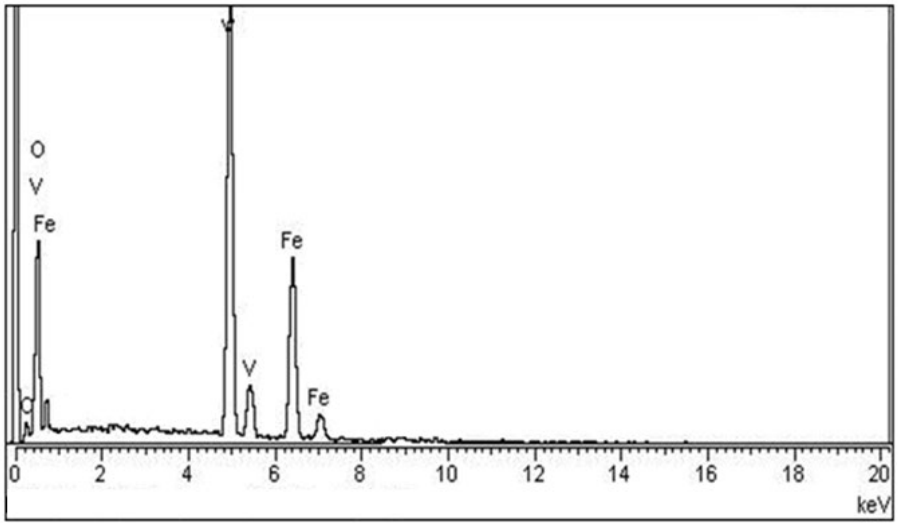

Fig. 2. EDX analysis of $FeVO_4$.

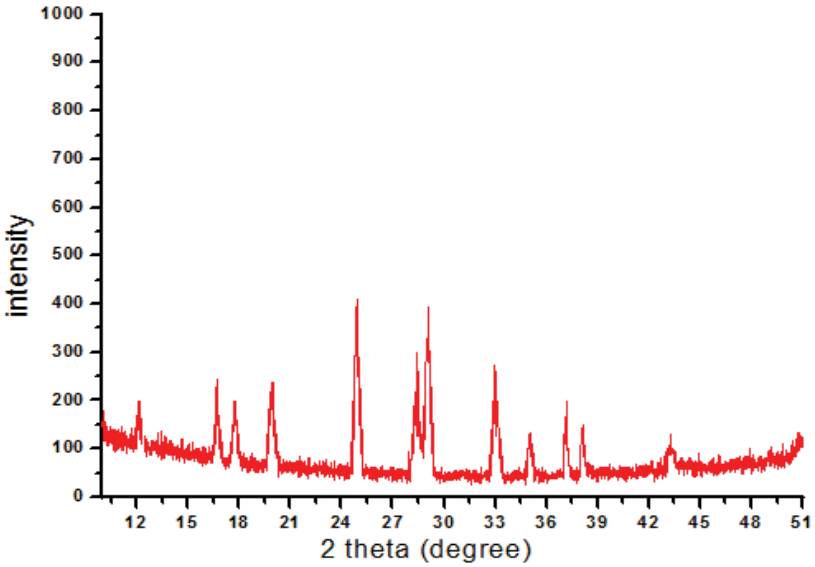

Fig. 3. XRD pattern of $FeVO_4$.

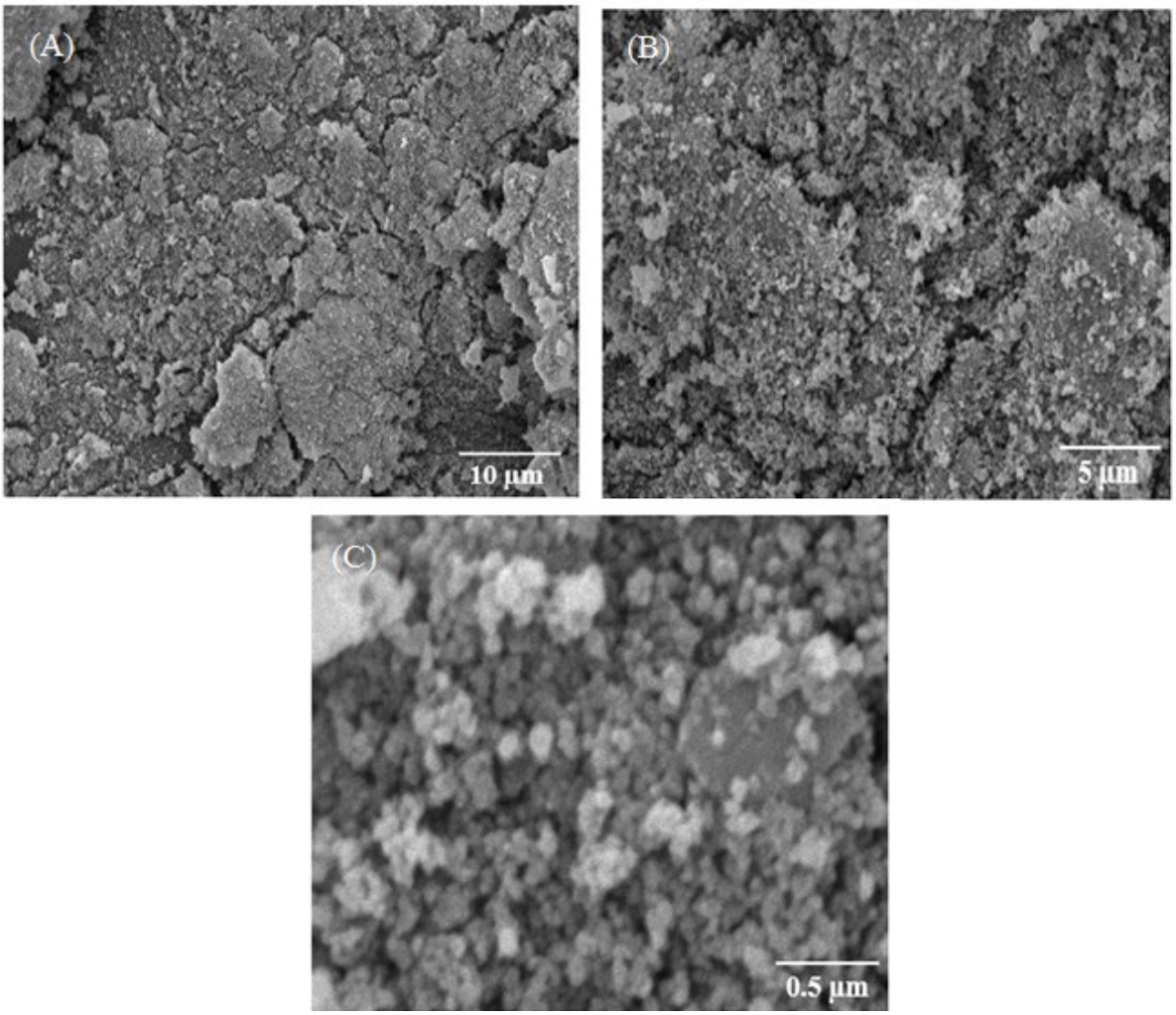

Fig. 4. SEM images of $FeVO_4$. Scale bar: (a) 10 µm, (b) 5 µm, and (c) 0.5 µm.

load were optimized using RSM and effect was evaluated on the basis of 2-CP degradation. It is quite evident from the results that the degradation process was affected significantly by the process variables and the observed vs. predicted degradation is shown in Table 2. The statistical analysis of the degradation data is shown in Tables 3 and 4. A sequential process was employed for model fitting and model summary statistics were utilized for the selection of model, while insignificant lack of fit test showed good predictability for the elaboration of the optimum response. Moreover, the adequacy of the model was further analyzed through analysis of variance (ANOVA) and based on *F* and *p*-values, the efficacy of the modal was evaluated. Larger *F*-value and smaller the value of *p* indicated that the model was suitable to ensure the optimal response [4,43]. Model fitting could be assessed through the determination of interaction between operational parameters in order to determine their effect on responses. *F*-value having 0.01 chances of noise ensures that the model is highly significant, all process variables are interdependent and have an effect on the PCA. Lower value of *F* calculated from ANOVA also ensures the role of different variables on the response [25,43]. The regression model also revealed that *A*, *B*, *C*, *D*, *AB*, *AD*, A^2, B^2, C^2, and D^2 values are significant, while other remaining interactions such as *BC*, *CD*, *BD*, and *AC* have an insignificant effect on the response with $P > 0.05$ (*A* = photocatalyst load, *B* = pH, *C* = 2-chlorophenol concentration, and *D* = H_2O_2 %). Furthermore, R^2-values 0.9993 for the quadratic model and 0.9996 for a cubic model with negligible deviation also indicated that the model was highly significant and insignificant lack of fit test indicated good predictability. Agreement of experimental values with predicted values showed the reliability of the CCD for optimization of process variables for the degradation of 2-CP. Optimized conditions for different operational variables were; 2 g/L catalyst load, pH 6, and 2-CP concentration 10 mg/L. For the verification of predicted values, an experiment was run under optimized conditions and the observed degradation value was found to be in concordant with the predicted results and 91% degradation of the 2-CP was achieved under optimum conditions. Contour diagrams showing the degradation of 2-CP can be seen in Figs. 7a–f. Percentage degradation of 2-CP was studied as a function of various process variables and it was observed that there exists a linear relationship between independent variables.

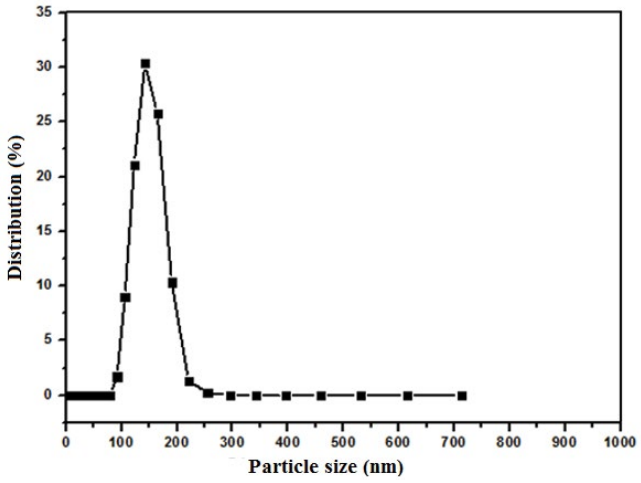

Fig. 5. Particle size distribution of $FeVO_4$.

3.2.1. Effect of photocatalyst dose on PCA

Catalyst dose is one of the important parameters in the photocatalytic process and optimum value is at the best to enhance the PCA at the lowest catalyst dose. so that an increase in catalyst concentration up to a certain limit enhanced the degradation, which is correlated with the generation of hydroxyl radicals [29], and beyond a certain dose of catalyst agglomeration may occur and PCA may reduce due to low penetration of the light [44]. Reduction in degradation rate by increasing the catalyst dose might be due to the possibility of higher recombination rate of electron to hole pair and also higher dosage than the optimum value might cause agglomeration which ultimately causes the poor penetration of light (Figs. 6a–c). The mechanism for the photocatalytic degradation of 2-CP is shown in Eqs. (3)–(6) [8,29,45,46].

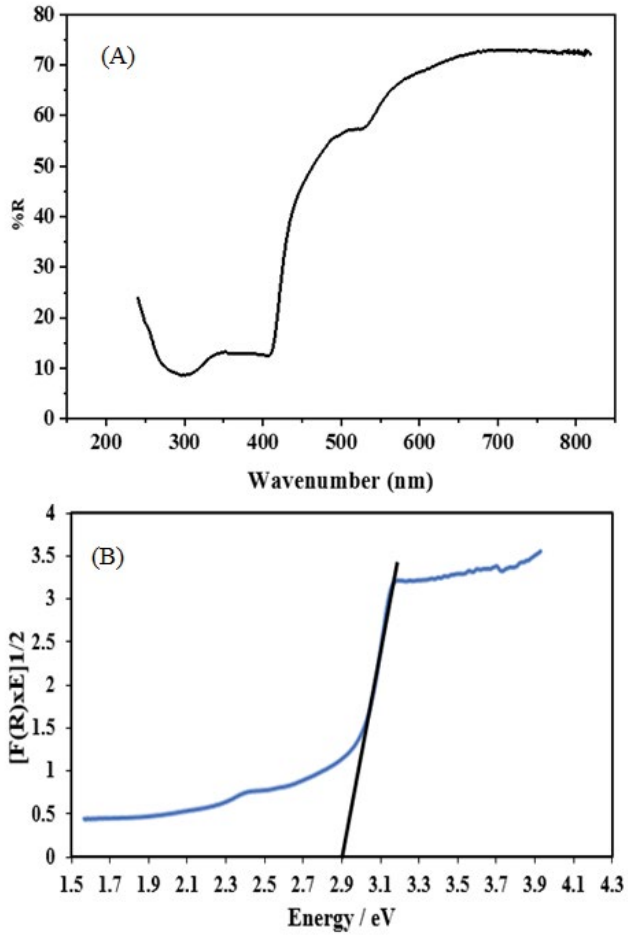

Fig. 6. (a) Diffused reflectance spectrum and (b) band gap energy of $FeVO_4$.

Table 3
Statistical analysis

(a) sequential model sum of squares [Type I] of model compound degraded by $FeVO_4$						
Source	Sum of square	*df*	Mean square	*F*-value	*p*-value	
Mean vs. total	66,080.19048	1	66,080.2			
Linear vs. mean	2,776.976354	4	694.244	2.80727	0.0611	
2FI vs. linear	161.8923115	6	26.9821	0.0711	0.998	
Quadratic vs. 2FI	3,790.489609	4	947.622	1,277.33	<0.0001	Suggested
Cubic vs. quadratic	1.651249422	2	0.82562	1.17946	0.3957	Aliased
Residual	2.8	4	0.7			
Total	72,814	21	3,467.33			

(b) Lack of fit (modal summary statistics)								
Source	Sum of squares	*df*	Mean square	Std. Dev.	*F*-value	PRESS	*p*-value	
Linear	3,954.03	12	329.503	15.7258	470.718	6,197.72	<0.0001	
2FI	3,792.14	6	632.023	19.4806	902.891	58,145.6	<0.0001	
Quadratic	1.65125	2	0.82562	0.86132	1.17946	197.955	0.3957	Suggested
Cubic	0	0		0.83666				Aliased
Pure error	2.8	4	0.7					

Quadratic $R^2 = 0.99934$, adj. $R^2 = 0.9978$, pred. $R^2 = 0.9706$; Cubic $R^2 = 0.99958$, adj. $R^2 = 0.99792$

Table 4
ANOVA of 2-CP degradation using $FeVO_4$

Source model	Sum of square	*df*	Mean square	*F*-value	*p*-value	
Model	6,729.36	14	480.668	647.9103766	<0.0001	significant
A-Photocatalyst load	0.5	1	0.5	0.673968074	0.4431	
B-pH	0.5	1	0.5	0.673968074	0.4431	
C-2-Chlorophenol	2,346.12	1	2,346.12	3,162.418157	<0.0001	
D-H_2O_2 (%)	128	1	128	172.535827	<0.0001	
AB	2.57681	1	2.57681	3.473376358	0.1116	
AC	28.125	1	28.125	37.91070417	0.0008	
AD	3.84865	1	3.84865	5.187737037	0.0630	
BC	21.125	1	21.125	28.47515113	0.0018	
BD	103.092	1	103.092	138.9612296	<0.0001	
CD	3.125	1	3.125	4.212300463	0.0860	
A^2	2,056.46	1	2,056.46	2,771.976129	<0.0001	
B^2	1,590.51	1	1,590.51	2,143.905692	<0.0001	
C^2	83.3438	1	83.3438	112.3421564	<0.0001	
D^2	583.877	1	583.877	787.0292647	<0.0001	
Residual	4.45125	6	0.74187			
Lack of fit	1.65125	2	0.82562	1.179463873	0.3957	insignificant
Pure error	2.8	4	0.7			
Cor. total	6,733.81	20				

$$FeVO_4 + hv \rightarrow h^+(VB) + e^-(CB) \quad (3)$$

$$O_2 + e^-CB \rightarrow O_2^{-\bullet} \quad (4)$$

$$h^+(VB) + H_2O \rightarrow {}^{\bullet}OH + {}^{\bullet}H + e_{aq} \quad (5)$$

$$^{\bullet}OH + 2\text{-CP} \rightarrow \text{Oxidative degradation} \quad (6)$$

$FeVO_4$ with various concentrations ranging from 1 to 3 g/L was employed to find out the optimum concentration at which the best efficiency can be achieved for the complete degradation of 2-CP. It was examined that lower

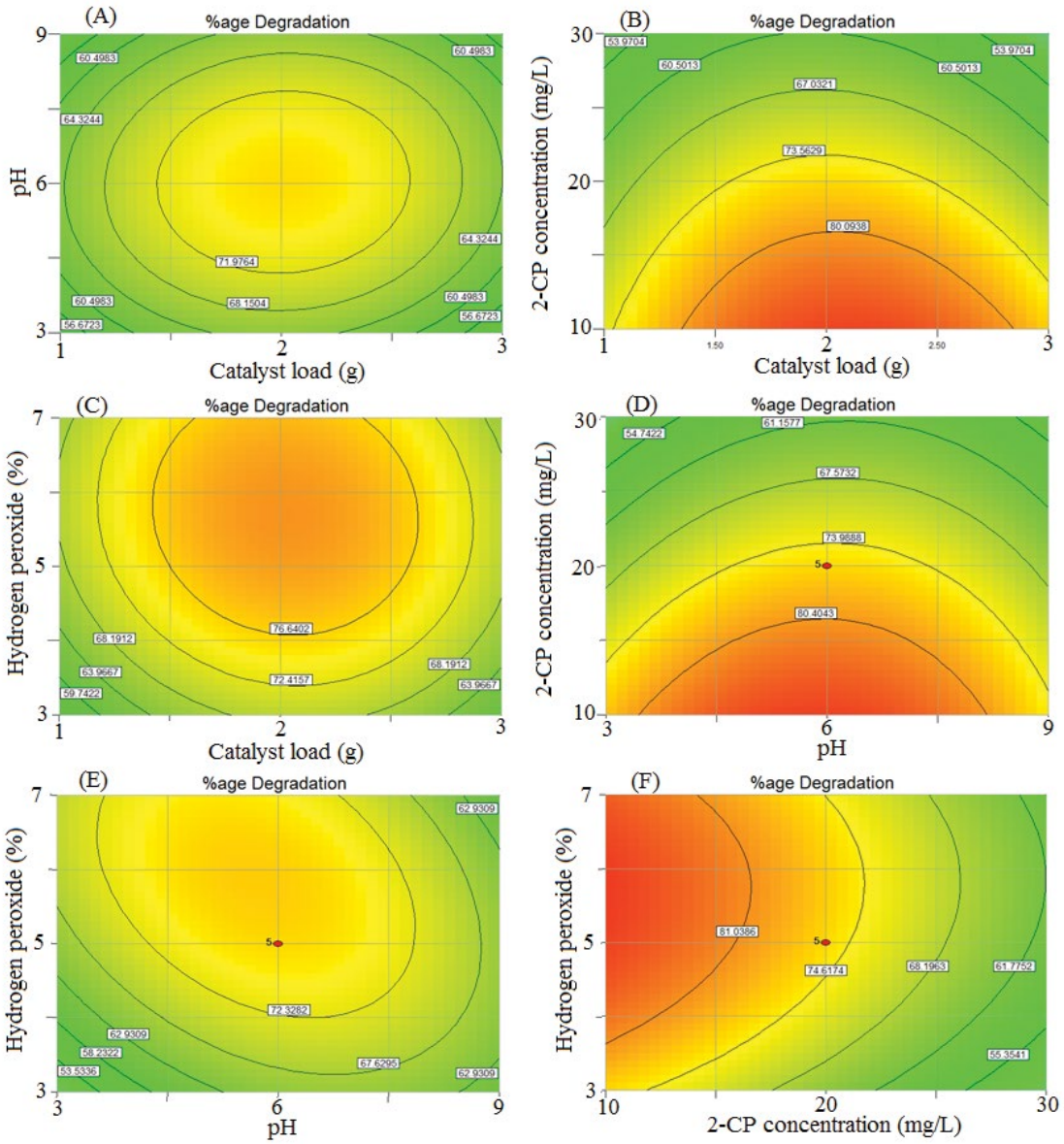

Fig. 7. Contour diagrams showing the degradation of 2-CP. (a) Catalyst load vs. pH, (b) Catalyst load vs. conc. of 2-chlorophenol, (c) Catalyst load vs. H_2O_2, (d) pH vs. conc. of 2-chlorophenol, (e) pH vs. H_2O_2, and (f) conc. of 2-chlorophenol vs. H_2O_2.

concentration of photocatalyst has no significant role in photodegradation, while degradation rate was increased by increasing the catalyst concentration and up to 91% degradation was attained at an optimum value of the catalyst

3.2.2. *Effect of pH*

Role of pH in photocatalytic degradation for complete mineralization of organic contaminants in wastewater is one of the important parameters. pH plays an effective role in degradation and detoxification of organic species, which creates electrostatic charge distribution upon the surface of photocatalyst which closely relates to catalytic activities on the surface. Protonation and deprotonation on the photocatalyst surface take place in the acidic or alkaline medium because of the charge bearing capacity of pH in different reaction media [25]. It was observed that $FeVO_4$ showed maximum degradation when the pH was 6 (Figs. 7a, d, and e) because mostly organic species either contain a basic nature or acidic behavior and their protonation or deprotonation takes place which is the reason for the generation of unstable species [47–49]. Electron hole pair formation mechanism is more predominant at suitable pH value which contributes toward the generation of more oxidizing species. It is concluded that protonation is more prominent at lower pH, which creates a positive charge on the catalyst surface causes enhanced catalytic process. Depletion of degradation process takes place in basic pH due to columbic repulsion forces because of the same charge distribution between positive charge species and photocatalyst.

3.2.3. Effect of 2-CP concentration

The degradation efficiency of the 2-CP was also studied by changing the initial concentration of 2-CP in the range of 10–30 mg/L. It was observed that the increase in the initial concentration of the 2-CP does not affect the degradation rate significantly. However, deactivation of the photocatalyst may occur due to the saturation of the active sites present on the catalyst surface which leads toward the low PCA and as the 2-CP concentration was increased, the reaction time was increased to ensure complete mineralization (Figs. 7b, d, and f).

3.3. Comparison of PCA of $FeVO_4$

PCA of $FeVO_4$ prepared and $FeVO_4$ commercial was compared by degrading of 2-CP. First samples were placed in the dark for adsorption of 2-CP on the material surface. Then, samples were irradiated for photocatalytic degradation of 2-CP and response are shown in Fig. 8 along with controls. It was observed that $FeVO_4$ prepared proved to be more effective catalyst as compared to commercial $FeVO_4$/commercial. The effect of light and H2O2 was negligible. Kinetic study of photocatalytic degradation of 2-CP was also examined by applying the Langmuir Hinshelwood (LH) model [50]. Relation of LH kinetic model for the rate constant of pseudo first order reaction is given in Eq. (7).

$$\ln\frac{C_0}{C} = k_1 t \tag{7}$$

where C_0 is the initial concentration of 2-CP, C is the concentration after treatment, t: time, and k_1: pseudo-first-order rate constant.

3.4. Degradation of product monitoring

High performance liquid chromatography (HPLC) was performed to monitor the degradation and by-product identification before and after treatment [51]. From the initial untreated sample, a clear distinct peak of 2-CP with a retention time of 6.313 min was obtained with an average peak area (764,456; Fig. 9). Reduction in peak area and peak intensity occurred in the treated 2-CP sample. A distinct peak with a retention time of 3.193 min was achieved after treating the sample. It is evident that after the attack of •OH, an alkyl chain is formed which on further oxidation changed into straight-chained alcohols which on further oxidation transformed to low molecular weight carboxylic acids and then finally to CO_2 and H_2O [13,27]. Results revealed that $FeVO_4$ based advanced oxidation process is viable to degrade 2-CP under solar light irradiation and under the current scenario of environmental pollution [52–62], there is a need to prepare and utilize materials able to harvest solar light for photocatalytic applications.

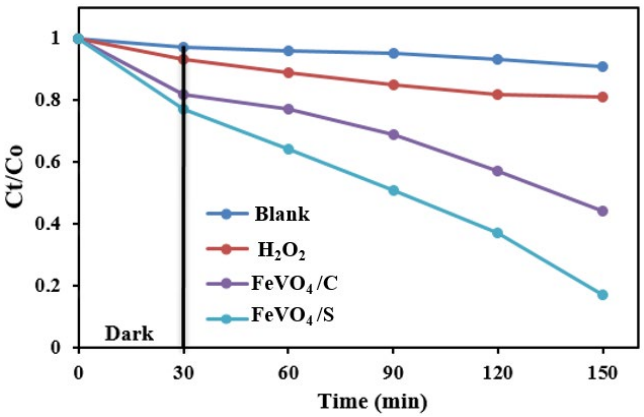

Fig. 8. Determination of photocatalytic degradation of 2-chlorophenol using synthesized and commercial $FeVO_4$ along with blanks.

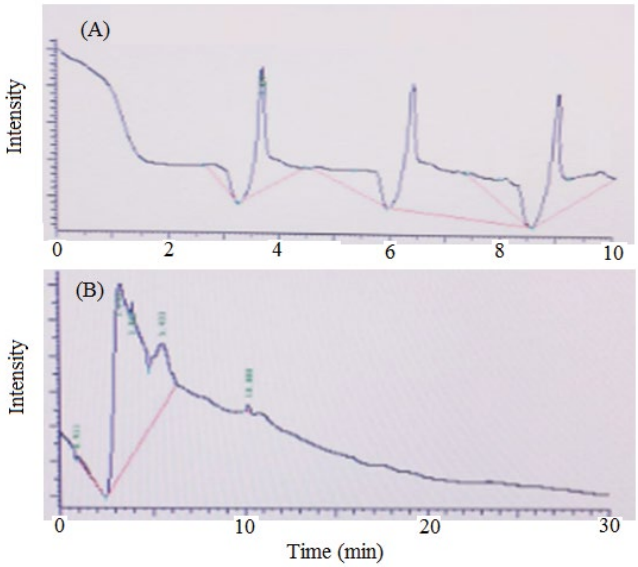

Fig. 9. HPLC chromatograms (a) untreated 2-chlorophenol and (b) treated sample of 2-chlorophenol.

4. Conclusions

In view of efficient PCA of heterostructured nanoparticles, $FeVO_4$ was prepared and characterized by advanced techniques. The average particle size was 150 nm. The $FeVO_4$ particle was spherical, fluffy and in aggregate form with a band-gap value of 2.95 eV. 2-CP was treated under solar light irradiation using $FeVO_4$ as a function of catalyst dose, pH, the concentration of 2-CP, H_2O_2 concentration. At optimum conditions of process variables, up to 91% degradation of 2-CP was achieved. The observed and predicted degradation of 2-CP degradation was in agreement with very low residual values. Results revealed that $FeVO_4$ is promising for the harvesting of solar light for photocatalytic applications to treat effluent containing 2-CP and related pollutants in wastewater.

Acknowledgment

Research work was funded by Endowment Fund Secretariat, University of Agriculture Faisalabad, Pakistan (Project identification No. 1553).

References

[1] G. Rytwo, T. Klein, S. Margalit, O. Mor, A. Naftali, G. Daskal, A continuous-flow device for photocatalytic degradation and full mineralization of priority pollutants in water, Desalin. Water Treat., 57 (2016) 16424–16434.

[2] M. Moradi, A.M. Mansouri, N. Azizi, J. Amini, K. Karimi, K. Sharafi, Adsorptive removal of phenol from aqueous solutions by copper (cu)-modified scoria powder: process modeling and kinetic evaluation, Desalin. Water Treat., 57 (2016) 11820–11834.

[3] S. Mohammadi, A. Kargari, H. Sanaeepur, K. Abbassian, A. Najafi, E. Mofarrah, Phenol removal from industrial wastewaters: a short review, Desalin. Water Treat., 53 (2015) 2215–2234.

[4] M.Z. Ahamd, S. Ehtisham-ul-Haque, N. Nisar, K. Qureshi, A. Ghaffar, M. Abbas, J. Nisar, M. Iqbal, Detoxification of photo-catalytically treated 2-chlorophenol: optimization through response surface methodology, Water Sci. Technol., 76 (2017) 323–336.

[5] M. Abbas, M. Adil, S. Ehtisham-ul-Haque, B. Munir, M. Yameen, A. Ghaffar, G.A. Shar, M.A. Tahir, M. Iqbal, *Vibrio fischeri* bioluminescence inhibition assay for ecotoxicity assessment: a review, Sci. Total Environ., 626 (2018) 1295–1309.

[6] M. Iqbal, *Vicia faba* bioassay for environmental toxicity monitoring: a review, Chemosphere, 144 (2016) 785–802.

[7] U. Kamran, H.N. Bhatti, M. Iqbal, A. Nazir, Green Synthesis of metal nanoparticles and their applications in different fields: a review, Z. Phys. Chem., 233 (2019) 1325–1349.

[8] I. Bibi, N. Nazar, S. Ata, M. Sultan, A. Ali, A. Abbas, K. Jilani, S. Kamal, F.M. Sarim, M.I. Khan, F. Jalal, M. Iqbal, Green synthesis of iron oxide nanoparticles using pomegranate seeds extract and photocatalytic activity evaluation for the degradation of textile dye, J. Mater. Res. Technol., 8 (2019) 6115–6124.

[9] M. Iqbal, M. Abbas, J. Nisar, A. Nazir, Bioassays based on higher plants as excellent dosimeters for ecotoxicity monitoring: a review, Chem. Int., 5 (2019) 1–80.

[10] M. Saeed, S. Adeel, M. Ilyas, M.A. Shahzad, M. Usman, E.-u. Haq, M. Hamayun, Oxidative degradation of Methyl Orange catalyzed by lab prepared nickel hydroxide in aqueous medium, Desalin. Water Treat., 57 (2016) 12804–12813.

[11] M. Bilal, M. Iqbal, H. Hu, X. Zhang, Mutagenicity and cytotoxicity assessment of biodegraded textile effluent by Ca-alginate encapsulated manganese peroxidase, Biochem. Eng. J., 109 (2016) 153–161.

[12] M. Bilal, M. Iqbal, H. Hu, X. Zhang, Mutagenicity, cytotoxicity and phytotoxicity evaluation of biodegraded textile effluent by fungal ligninolytic enzymes, Water Sci. Technol., 73 (2016) 2332–2344.

[13] M. Iqbal, I.A. Bhatti, Gamma radiation/H_2O_2 treatment of a nonylphenol ethoxylates: degradation, cytotoxicity, and mutagenicity evaluation, J. Hazard. Mater., 299 (2015) 351–360.

[14] H.N. Bhatti, A. Jabeen, M. Iqbal, S. Noreen, Z. Naseem, Adsorptive behavior of rice bran-based composites for malachite green dye: isotherm, kinetic and thermodynamic studies, J. Mol. Liq., 237 (2017) 322–333.

[15] V.R. Remya, V.K. Abitha, P.S. Rajput, A.V. Rane, A. Dutta, Silver nanoparticles green synthesis: a mini review, Chem. Int., 3 (2017) 165–171.

[16] O.U. Igwe, F. Nwamezie, Green synthesis of iron nanoparticles using flower extract of *Piliostigma thonningii* and antibacterial activity evaluation, Chem. Int., 4 (2018) 60–66.

[17] L.S. Al Banna, N.M. Salem, A.M. Awwad, Green synthesis of sulfur nanoparticles using *Rosmarinus officinalis* leaves extract and anti-nematicidal activity against *Meloidogyne javanica*, Chem. Int., 6 (2020) 137–143.

[18] A.M. Awwad, N.M. Salem, M.M. Aqarbeh, F.M. Abdulaziz, Green synthesis, characterization of silver sulfide nanoparticles and antibacterial activity evaluation, Chem. Int., 6 (2020) 42–48.

[19] S. Şaşmaz, S. Gedikli, P. Aytar, G. Güngörmedi, A. Çabuk, E. Hür, A. Ünal, N. Kolankaya, Decolorization potential of some reactive dyes with crude laccase and laccase-mediated system, Appl. Biochem. Biotechnol., 163 (2011) 346–361.

[20] M. Sasmaz, B. Akgul, D. Yıldırım, A. Sasmaz, Bioaccumulation of thallium by the wild plants grown in soils of mining area, Int. J. Phytorem., 18 (2016) 1164–1170.

[21] M. Sasmaz, E. Obek, A. Sasmaz, Bioaccumulation of uranium and thorium by lemna minor and lemna gibba in Pb-Zn-Ag tailing water, Bull. Environ. Contam. Toxicol., 97 (2016) 832–837.

[22] A.M. Alasadi, F.I. Khaili, A.M. Awwad, Adsorption of Cu(II), Ni(II) and Zn(II) ions by nano kaolinite: thermodynamics and kinetics studies, Chem. Int., 5 (2019) 258–268.

[23] M.M. Alaqarbeh, M.W. Shammout, A.M. Awwad, Nano platelets kaolinite for the adsorption of toxic metal ions in the environment, Chem. Int., 6 (2020) 49–55.

[24] A.M. Alkherraz, A.K. Ali, K.M. Elsherif, Removal of Pb(II), Zn(II), Cu(II) and Cd(II) from aqueous solutions by adsorption onto olive branches activated carbon: equilibrium and thermodynamic studies, Chem. Int., 6 (2020) 11–20.

[25] K. Qureshi, M.Z. Ahmad, I.A. Bhatti, M. Zahid, J. Nisar, M. Iqbal, Graphene oxide decorated $ZnWO_4$ architecture synthesis, characterization and photocatalytic activity evaluation, J. Mol. Liq., 285 (2019) 778–789.

[26] S.-S. Chang, S.O. Yoon, H.J. Park, A. Sakai, Luminescence properties of Zn nanowires prepared by electrochemical etching, Mater. Lett., 53 (2002) 432–436.

[27] M. Iqbal, J. Nisar, M. Adil, M. Abbas, M. Riaz, M.A. Tahir, M. Younus, M. Shahid, Mutagenicity and cytotoxicity evaluation of photo-catalytically treated petroleum refinery wastewater using an array of bioassays, Chemosphere, 168 (2017) 590–598.

[28] U. Kamran, H.N. Bhatti, M. Iqbal, S. Jamil, M. Zahid, Biogenic synthesis, characterization and investigation of photocatalytic and antimicrobial activity of manganese nanoparticles synthesized from *Cinnamomum verum* bark extract, J. Mol. Struct., 1179 (2019) 532–539.

[29] S. Ata, I. Shaheen, S. Ghafoor, M. Sultan, F. Majid, I. Bibi, M. Iqbal, Graphene and silver decorated ZnO composite synthesis, characterization and photocatalytic activity evaluation, Diamond Relat. Mater., 90 (2018) 26–31.

[30] M. Rahmat, A. Rehman, S. Rahmat, H.N. Bhatti, M. Iqbal, W.S. Khan, Y. Jamil, S.Z. Bajwa, Y. Sarwar, S. Rasul, Laser ablation assisted preparation of MnO_2 nanocolloids from waste battery cell powder: evaluation of physico-chemical, electrical and biological properties, J. Mol. Struct., 1191 (2019) 284–290.

[31] M. Arshad, M. Abbas, S. Ehtisham-ul-Haque, M.A. Farrukh, A. Ali, H. Rizvi, G.A. Soomro, A. Ghaffar, M. Yameen, M. Iqbal, Synthesis and characterization of SiO_2 doped Fe_2O_3 nanoparticles: photocatalytic and antimicrobial activity evaluation, J. Mol. Struct., 1180 (2019) 244–250.

[32] M. Arshad, A. Qayyum, G. Abbas, R. Haider, M. Iqbal, A. Nazir, Influence of different solvents on portrayal and photocatalytic activity of tin-doped zinc oxide nanoparticles, J. Mol. Liq., 260 (2018) 272–278.

[33] M. Arshad, A. Qayyum, G.A. Shar, G.A. Soomro, A. Nazir, B. Munir, M. Iqbal, Zn-doped SiO_2 nanoparticles preparation and characterization under the effect of various solvents: antibacterial, antifungal and photocatlytic performance evaluation, J. Photochem. Photobiol. B, 185 (2018) 176–183.

[34] M. Ghiyasiyan-Arani, M. Salavati-Niasari, S. Naseh, Enhanced photodegradation of dye in waste water using iron vanadate nanocomposite; ultrasound-assisted preparation and characterization, Ultrason. Sonochem., 39 (2017) 494–503.

[35] V. Nithya, R.K. Selvan, C. Sanjeeviraja, D.M. Radheep, S. Arumugam, Synthesis and characterization of $FeVO_4$ nanoparticles, Mater. Res. Bull., 46 (2011) 1654–1658.

[36] S. Hosseinpour-Mashkani, A. Sobhani-Nasab, M. Maddahfar, Synthesis, characterization and investigation magnetic and photovoltaic properties of $FeVO_4$ nanoparticles, J. Nanostruct., 6 (2016) 70–73.

[37] B.D. Cullity, S.R. Stock, Elements of X-ray Diffraction, Pearson Education, Uttar Pradesh, India, 2014.

[38] J. Deng, J. Jiang, Y. Zhang, X. Lin, C. Du, Y. Xiong, $FeVO_4$ as a highly active heterogeneous Fenton-like catalyst towards the degradation of Orange II, Appl. Catal. B, 84 (2008) 468–473.

[39] S.H.S. Chan, T. Yeong Wu, J.C. Juan, C.Y. Teh, Recent developments of metal oxide semiconductors as photocatalysts in advanced oxidation processes (AOPs) for treatment of dye waste-water, J. Chem. Technol. Biotechnol., 86 (2011) 1130–1158.
[40] B. Ozturk, G.S.P. Soylu, Synthesis of surfactant-assisted $FeVO_4$ nanostructure: characterization and photocatalytic degradation of phenol, J. Mol. Catal. A, 398 (2015) 65–71.
[41] H. Ma, X. Yang, Z. Tao, J. Liang, J. Chen, Controllable synthesis and characterization of porous $FeVO_4$ nanorods and nanoparticles, CrystEngComm., 13 (2011) 897–901.
[42] D.S. Bhatkhande, V.G. Pangarkar, A.A.C.M. Beenackers, Photocatalytic degradation for environmental applications–a review, J. Chem. Technol. Biotechnol., 77 (2002) 102–116.
[43] M. Iqbal, N. Iqbal, I.A. Bhatti, N. Ahmad, M. Zahid, Response surface methodology application in optimization of cadmium adsorption by shoe waste: a good option of waste mitigation by waste, Ecol. Eng., 88 (2016) 265–275.
[44] A. Ashar, M. Iqbal, I.A. Bhatti, M.Z. Ahmad, K. Qureshi, J. Nisar, I.H. Bukhari, Synthesis, characterization and photocatalytic activity of ZnO flower and pseudo-sphere: nonylphenol ethoxylate degradation under UV and solar irradiation, J. Alloys Compd., 678 (2016) 126–136.
[45] I. Bibi, S. Kamal, A. Ahmed, M. Iqbal, S. Nouren, K. Jilani, N. Nazar, M. Amir, A. Abbas, S. Ata, F. Majid, Nickel nanoparticle synthesis using *Camellia Sinensis* as reducing and capping agent: growth mechanism and photo-catalytic activity evaluation, Int. J. Biol. Macromol., 103 (2017) 783–790.
[46] N. Nazar, I. Bibi, S. Kamal, M. Iqbal, S. Nouren, K. Jalani, M. Umair, S. Atta, Cu nanoparticles synthesis using biological molecule of *P. granatum* seeds extract as reducing and capping agent: growth mechanism and photo-catalytic activity, Int. J. Biol. Macromol., 106 (2017) 1203–1210.
[47] A. Jamil, T.H. Bokhari, M. Iqbal, I.A. Bhatti, M. Zuber, J. Nisar, N. Masood, Gamma radiation and hydrogen peroxide based advanced oxidation process for the degradation of disperse dye in aqueous medium, Z. Phys. Chem., 234 (2020) 279–294, doi: 10.1515/zpch-2019–1384
[48] A. Jamil, T.H. Bokhari, M. Iqbal, M. Zuber, I.H. Bukhari, ZnO/UV/H_2O_2 based advanced oxidation of disperse red dye, Z. Phys. Chem., 234 (2020) 129–143, doi: 10.1515/zpch-2019–0006
[49] A. Jamil, T.H. Bokhari, T. Javed, R. Mustafa, M. Sajid, S. Noreen, M. Zuber, A. Nazir, M. Iqbal, M.I. Jilani, Photocatalytic degradation of disperse dye Violet-26 using TiO_2 and ZnO nanomaterials and process variable optimization, J. Mater. Res. Technol., 9 (2020) 1119–1128, doi: 10.1016/j.jmrt.2019.1011.1035
[50] C.T. Campbell, S.-K. Shi, J. White, The Langmuir-Hinshelwood reaction between oxygen and CO on Rh, Appl. Surf. Sci., 2 (1979) 382–396.
[51] N.A. Ayofe, P.O. Oladoye, D.O. Jegede, Extraction and quantification of phthalates in plastic coca-cola soft drinks using high performance liquid chromatography (HPLC), Chem. Int., 4 (2018) 85–90.
[52] S. Mansouri, N. Elhammoudi, S. Aboul-hrouz, M. Mouiya, L. Makouki, A. Chham, A. Abourriche, H. Hannache, M. Oumam, Elaboration of novel adsorbent from Moroccan oil shale using Plackett–Burman design, Chem. Int., 4 (2018) 7–14.
[53] N.E. Ibisi, C.A. Asoluka, Use of agro-waste (*Musa paradisiaca* peels) as a sustainable biosorbent for toxic metal ions removal from contaminated water, Chem. Int., 4 (2018) 52–59.
[54] S. Ghezali, A. Mahdad-Benzerdjeb, M. Ameri, A.Z. Bouyakoub, Adsorption of 2,4,6-trichlorophenol on bentonite modified with benzyldimethyltetradecylammonium chloride, Chem. Int., 4 (2018) 24–32.
[55] M. Fazal-ur-Rehman, Methodological trends in preparation of activated carbon from local sources and their impacts on production: a review, Chem. Int., 4 (2018) 109–119.
[56] A. Sasmaz, S. Ozkan, M.F. Gursu, M. Sasmaz, The hematological and biochemical changes in rats exposed to britholite mineral, Appl. Radiat Isot., 129 (2017) 185–188.
[57] M. Sasmaz, A. Sasmaz, The accumulation of strontium by native plants grown on Gumuskoy mining soils, J. Geochem. Explor., 181 (2017) 236–242.
[58] M. Palutoglu, B. Akgul, V. Suyarko, M. Yakovenko, N. Kryuchenko, A. Sasmaz, Phytoremediation of cadmium by native plants grown on mining soil, Bull. Environ. Contam. Toxicol., 100 (2018) 293–297.
[59] O. Chidi, R. Kelvin, Surface interaction of sweet potato peels (*Ipomoea batata*s) with Cd(II) and Pb(II) ions in aqueous medium, Chem. Int., 4 (2018) 221–229.
[60] A. Chham, E. Khouya, M. Oumam, A.K. Abourriche, S. Gmouh, M. larzek, S. Mansouri, N. Elhammoudi, N. Hanafi, H. Hannache, The use of insoluble mater of Moroccan oil shale for removal of dyes from aqueous solution, Chem. Int., 4 (2018) 67–76.
[61] F.O. Abulude, D.N. Ogunmola, M.M. Alabi, Y. Abdulrasheed, Atmospheric deposition: effects on sculptures, Chem. Int., 4 (2018) 136–145.
[62] G. Abbas, I. Javed, M. Iqbal, R. Haider, F. Hussain, N. Qureshi, Adsorption of non-steroidal anti-inflammatory drugs (diclofenac and ibuprofen) from aqueous medium onto activated onion skin, Desalin. Water Treat., 95 (2017) 274–285.